



Enhanced electrochemical response of carbon quantum dot modified electrodes



M. Algarra^{a,*}, A. González-Calabuig^b, K. Radotić^c, D. Mutavdzic^c, C.O. Ania^d,
J.M. Lázaro-Martínez^e, J. Jiménez-Jiménez^a, E. Rodríguez-Castellón^a, M. del Valle^{b,*}

^a Departamento de Química Inorgánica, Facultad de Ciencias, Universidad de Málaga, Campus de Teatinos s/n, 29071 Málaga, Spain

^b Sensors and Biosensors Group, Chemistry Department, Universitat Autònoma de Barcelona, 08193 Bellaterra, Barcelona, Spain

^c Institute for Multidisciplinary Research, University of Belgrade, Kneza Višeslava 1, 11000 Beograd, Serbia

^d CEMHTI (UPR 3079), CNRS, Univ. Orléans, 45071 Orléans, France

^e Universidad de Buenos Aires, IQUIFIB-CONICET, Facultad de Farmacia y Bioquímica, Departamento de Química Orgánica, Junín 956 (1113), CABA, Argentina

ARTICLE INFO

Keywords:

Modified electrode
Voltammetry
Carbon dot
Nanomaterial

ABSTRACT

A glassy carbon electrode (GCE) was surface-modified with carbon quantum dots (CQDs) and applied for the effective enhancement of the electrochemical signal for dopamine and uric acid determination. CQDs were prepared from graphite by a green modification of the Hummers method. They were characterized by FTIR-ATR, XPS, solid-state NMR, fluorescence and Raman spectroscopies. TPD-MS analysis was applied to characterize the functionalization of the surface. The CQDs were assembled on the glassy carbon electrode by adsorption because of the large number of carboxy groups on their surface warrants effective adsorption. The modified GCE exhibits a sensitivity that is almost 10 times better than of the bare GCE. The lower limits of detection are 1.3 μM for uric acid and 2.7 μM for dopamine.

1. Introduction

Carbon quantum dots (CQDs) have created immense interest to the research community since their discovery in 2004 [1]. CQDs offer a strong potential to replace traditional semiconductor quantum dots because of their unique luminescence performance, their smaller size, their high photostability against photo-bleaching and blinking [2], their biocompatibility and their low toxicity [3,4]. Taking the advantage of abundant content in the earth, carbon based materials have emerged as attractive candidates for the development of bio-imaging, medical diagnosis, catalysis, photovoltaic and many other users in optoelectronic devices [5–11].

CQDs are obtained by a wide variety of methods, traditional well known as top-down and bottom-up approaches, which can be improved during preparation or post-treatment [12]. CQDs obtained from graphite or graphite oxides, under the frame of top-down procedures, have emerged as an interesting procedure to dispose of them. Their internal C linkage by sp^2 confers the chemical ability to be converted in smallest units, which under oxidation process can be converted in CQDs. These oxidations are mainly in the surface, leading the origin of their main properties which are currently under deeper analysis.

Concerning the chemical characterization of graphite oxide

materials, only a few spectroscopic methods, such as FTIR, Raman and NMR, may bring substantially chemical information related with the bulk structure [13–15]. Thus, solid-state NMR (*ss*-NMR) experiments are used to analyze in detail the chemical structure of non-soluble materials in general. Especially, *ss*-NMR spectroscopy has progressively evolved into a cornerstone technique for the characterization of an impressively broad range of materials [16,17]. In addition, *ss*-NMR has the advantage of retrieving information in a non-invasive way and without the need of modifying the samples. However, for studying modified graphite oxide it is necessary to applied different ^{13}C cross polarization and magic angle spinning (CP-MAS), ^{13}C CP-MAS combined with dipolar dephasing and direct ^{13}C pulse experiments, among others, in order to maximize the information that can be obtained through *ss*-NMR.

Being hot topic in optical applications, CQDs have remained as a secondary carbon material in the field of analytical electrochemistry as the main characteristic employed for sensing are their luminescent properties [18]. Although there is little research in the integration of quantum dots in electrochemical sensors, some authors have integrated CQDs into these. A CQDs-chitosan film onto a glassy carbon electrode has been reported to increase its electrochemical performance, in this case the determination of dopamine [19]. It has also been reported the

* Corresponding authors.

E-mail addresses: malgarra67@gmail.com (M. Algarra), manel.delvalle@gmail.com (M. del Valle).

comparison of graphene quantum dots and CQDs surface modifications of basal-plane pyrolytic graphite electrodes, indicating that the CQDs may have some different and interesting catalytic properties [20], even if compared with fluorescence detection [21].

The present work reports the modification of glassy carbon electrodes with CQDs which were synthesized and characterized for this purpose; electrochemical sensors prepared have been evaluated for dopamine and uric acid determination and the results compared with previous works in the literature.

2. Experimental

2.1. Chemicals and materials

Graphite (2 H type) was obtained by exfoliation of a commodity pencil. Potassium permanganate (KMnO_4 , > 99.0%), hydrofluoric acid (HF, 48 wt% in H_2O) and hydrogen peroxide (H_2O_2 , 30%) were purchased from Merck (Darmstadt, Germany). Deionized water with resistivity higher than 4 $\text{M}\Omega\text{ cm}$ was used.

2.2. Synthesis of Carbon quantum dots

CQDs were prepared by means a modification of the well-known Hummers method [22]. Pencil graphite (1 g) was dispersed uniformly in concentrated HF (50 mL), in which was dissolved KMnO_4 (6 g), and then the mixture was treated under reflux at 90 °C for 1 h in a Teflon reactor. Afterwards, it was left to cool down naturally and H_2O_2 (10 mL) was added. The resulted dark brown suspension was diluted with H_2O and centrifuged at 3000 rpm for 15 min to separate the less-fluorescent deposit, and dried at 90 °C, exhibiting a strong fluorescent powder (CQDs) under UV light.

2.3. Characterization techniques

The electron microscopy study was performed in transmission mode (TEM) using a JEM 1010 microscope (JEOL, Japan; 80 kV) equipped with a digital camera (Olympus, Megaview II). Fourier Transform-Infrared (FTIR) and attenuated total reflection (ATR) spectra were recorded on a Spectrum 1000 Perkin-Elmer spectrometer using KBr pellets. Raman measurements were carried out on a Senterra dispersive Raman spectrometer (Bruker with 532 nm as excitation). The back Raman scattering was collected with a standard spectral resolution of 3 cm^{-1} , spatial resolution of 0.5 mm, and spot size of about 3 mm. X-ray photoelectron spectroscopic (XPS) was performed on a Physical Electronic PHI 5700 spectrometer using non-monochromatic Mg- K_{α} radiation (300 W, 15 kV and 1253.6 eV) for analyzing the core-level signals of the elements of interest with a hemispherical multichannel detector. The spectra of powdered samples were recorded with a constant pass energy value at 29.35 eV, using a 720 μm diameter circular analysis area. The X-ray photoelectron spectra obtained were analyzed using PHI ACCESS ESCA-V6.0 F software and processed using MultiPak 8.2B package. The binding energy values were referenced to adventitious carbon C 1 s signal (284.8 eV). Shirley-type background and Gauss-Lorentz curves were used to determine the binding energies. The zeta potential (ζ) of CQDs was determined using a Zetasizer Nano ZS (Malvern Instruments, U.K.) equipped with a 4 mW HeNe laser operating at $\lambda = 633\text{ nm}$. ζ measurements were performed at 25 °C in polycarbonate folded capillary cells, incorporated with Au plated electrodes (DTS1061) and deionized H_2O was the dispersion medium. ζ was automatically obtained by the software, using the Stokes-Einstein and the Henry equation, with the Smoluchowski approximation. Fluorescence Spectroscopy and Data Analysis spectra of graphite and corresponding CQDs were collected using an FL3-221P spectrofluorimeter (JobinYvon Horiba, Paris, France) equipped with a 450 W Xe lamp and a photomultiplier tube. The spectra of CQDs compound were measured in the front-face configuration of the measuring cavity.

The slits on the excitation and emission beams were fixed both at 2 nm. The integration time was 0.1 s. The spectra were corrected for dark counts. The Rayleigh masking was applied in order to reduce Rayleigh scattering from the solid sample which limits the sensitivity and accuracy of the measurement. For each compound a series of 21 emission spectra was collected, by excitation at different wavelengths. The excitation range was 420–480 nm, with 3 nm step. The emission spectra were measured in the range 600–650 nm, with 1 nm increment. In the analysis, we used matrix, corresponding to the CQDs emission spectra. The matrix was analyzed by using Multivariate Curve Resolution-Alternating Least Squares (MCR-ALS) method [23], which extracted the number of components, as well as their emission profiles. All analyses were performed using The Unscrambler software package (Camo ASA). Electrochemical measurements were performed at room temperature (25 °C) using a $\mu\text{STAT}200$ potentiostat from Dropsens (Oviedo, Spain) using Dropview (Dropsens) software for data acquisition and control of the experiments. A three electrode cell configuration was employed; it was formed by a glassy carbon disk electrode (CH Instruments, Inc., Austin, USA) as the working electrode and a combination electrode formed by a Pt disk and a Ag/AgCl reference electrode (Crison 5261, Barcelona, Spain) as counter and reference electrodes, respectively. Temperature programmed desorption (TPD) measurements were recorded in a chemisorption analyzer (Autochem 292) connected to a mass spectrometer for gas analysis. About 40 mg of carbon sample were heated up to 900 °C (10 °C min^{-1}) under a constant helium flow (50 mL min^{-1}). The equipment is coupled to a mass spectrometer that allows the analysis and quantification of the desorbed gaseous products. The gas evolution profiles as a function of temperature were obtained and deconvoluted to estimate the different surface groups according to their corresponding desorption temperatures [24,25]. Solid-state NMR (*ss-NMR*) experiments were performed at room temperature in a Bruker Avance II-300 spectrometer equipped with a 4-mm MAS probe or in a Bruker Avance III HD Ascend 600 MHz spectrometer equipped with a 3.2-mm MAS probe. The operating frequency for protons and carbons was 300.13 and 75.46 MHz or 600.09 and 150.91 MHz, respectively. Glycine was used as an external reference for the ^{13}C spectra and to set the Hartmann-Hahn matching condition in the cross-polarization experiments in ^{13}C spectra. ^{13}C natural abundance direct polarization experiments with proton decoupling (SPINAL64) [26] during acquisitions were conducted for all the samples. An excitation pulse of 4.0 μs and a recycling time of 50 s was used and 40,000 scans were accumulated in order to obtain good signal to noise ratio. The spinning rate for all the samples was 10 or 15 kHz.

2.4. Electrochemical application of the sensor

In order to modify the original electrode with CQDs a suspension of 1 mg mL^{-1} of the obtained nanomaterial was prepared in water. This suspension was sonicated thoroughly during 2 h for a proper dispersion of the nanoparticles, then 40 μL of the suspension were deposited in the glassy carbon surface and dried at 40 °C for 1 h. All measured samples were prepared in PBS (50 mM) and KCl (100 mM) at pH 7. The voltammetric technique employed was linear sweep voltammetry, a linear voltammogram was recorded for each sample by measuring the current between 0.0 V and +1.1 V vs. Ag/AgCl with a step potential of 9 mV and a scan rate of 100 mV s^{-1} .

3. Results and discussion

3.1. Synthesis and characterization of CQDs

The synthetic route performed for the fabrication of CQDs from graphite was based on a deeply modification of the Hummer's method [22] as detailed in the experimental section. This allows avoiding the formation of gaseous impurities, retrieving a fluorescent material that indicates the presence of CQDs.

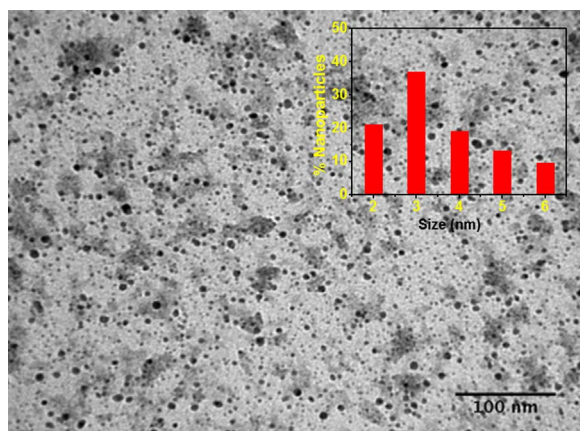


Fig. 1. TEM image of CQDs obtained from the graphite (inset, size distribution of ca. 270 nanoparticles).

An extensive characterization was performed on the resulting carbon material to further confirm the presence of carbon quantum dots with this process. Fig. 1 displays TEM images of the prepared CQDs, showing the size and morphology of the nanoparticles. As seen, the CQDs displayed nearly spherical size and a monodispersed distribution of sizes of average diameter about ca. 3.3 nm (inset in Fig. 1).

The oxidation procedure carried out on the graphite yielded a relative negative electrostatic charge at the CQDs/water interface, as evidenced by the zeta potential value ($\zeta = -16.76 \pm 0.51$ mV) a indicative of the presence of ionizable functional groups (ca. -OH and/or -COOH). In Supplementary information (Fig. S1A) is shown the FTIR spectrum of the graphite after oxidation and the CQDs, with both materials presenting quite similar profiles. In the case of the CQDs various bands indicate the presence of oxygen functionalities of varied nature. The bands at 3422 , 1724 and 1630 cm^{-1} are assigned to O-H stretching vibrations, the stretching vibrations related to C=O from COOH, and the skeletal vibrations of un-oxidized graphitic domains, respectively. Additionally, the characteristic peaks at 1035 and 1153 cm^{-1} for C-O / C-OH stretching vibrations in the plane of hydroxyl or epoxy groups [27] were also detected. The presence of peaks at 2917 cm^{-1} (sym) and 2842 cm^{-1} (asym) confirmed the presence of aliphatic CH_2 groups, and the band at 1464 cm^{-1} is attributed to the deformation of the C=C bond. Peaks below 900 cm^{-1} are not usually interpreted because they represent too complex a structural signature, but the presence of a sharp and strong peak at 731 cm^{-1} can be assigned to the presence of stretching mode of C-F bonds [28].

Further information on the structure of the CQDs was obtained from Raman spectroscopy. As seen in Fig. S1B, the spectrum of the pristine pencil graphite precursor showed the expected profile of a graphite, with a narrow G band in the first order spectra at 1589 cm^{-1} corresponding to the stretching E_{2g} vibration mode of the aromatic sp^2 carbon atoms [29], and a small contribution at 1349 cm^{-1} due to the breathing mode of sp^2 rings (defects in the aromatic sp^2 layers). The peaks of the second order spectrum are well-defined in both cases. No significant differences are observed between the Raman spectra of the pencil and the CDS, as already observed for other similar materials [30]. The intensity of the D band, related to the size of the in-plane sp^2 domains [31], slightly increased for the CQDs. However, the I_D/I_G values ranged from 3.2 for the graphite to 6.2 for the CQDs, which pointed to highly ordered crystal structures arising from large sp^2 clusters.

The comparison of the survey XPS spectra of both materials is shown in Fig. 2A, and clear differences are seen. The high-resolution spectra of C 1s demonstrate the obvious changes in carbon chemical environments from graphite to CQDs (Fig. 2B-C).

The C 1s core level spectrum of graphite is very complex (Fig. 2B) and can be decomposed in several contributions at 284.8 (34%), 286.2 (18%), 287.3 (25%), 288.5 (15%), 289.7 (6%) and 291.4 eV (2%).

These contributions are assigned to C=C/C-C/adventitious carbon (284.8 eV), C-OH/C-O-C (286.2 eV), C=O (287.3 eV), O=C-O (288.5 eV), carbonates (289.7 eV) and $\pi \rightarrow \pi^*$ transitions (291.4 eV). However, the C1s core level spectrum of CQDs only shows a dominant graphitic contribution at 284.8 eV (arising from C=C/C-C) and a weak contribution at 287.9 eV (O=C-OH) (Fig. 2C), typically of graphenoid structure [32]. The strong F1s peak at 686.4 eV (Fig. S2) is mainly due to the formation of silicon fluoride compounds [33]. Meanwhile the O 1s peak at ca. 531.5 eV is assigned to carbonyl (C=O). The O/C atomic ratios in graphite and CQDs are 0.15 and 0.13, respectively. It is important to point out that the XPS spectra of the obtained CQDs prepared by exfoliation of graphite is similar to that reported for graphite oxide [34].

With the idea of characterizing the chemical structure of the CQDs, ss-NMR experiments were performed and the results are shown in Fig. 3. The ^{13}C CP-MAS spectra with different contact times from 100 μs to 6 ms did not arise resonance signals after three days of measurement; this may be due to the low density of protons in the CQDs particles together with a higher content of amorphous component in comparison with the ordered structure in graphite since the CP-MAS experiment increase carbon signal coming from ordered region [35]. For that reason, ^{13}C direct polarization experiments (^{13}C DP) were done in order get some insights about the chemical structure regarding the functional groups present after the treatment of the graphite. One problem that arose for the study of graphite and related materials is the acquisition of solid-state ^{13}C NMR spectra under the magic angle spinning with a good signal-to-noise (S/N) ratio for non-labeled ^{13}C samples. In addition, some background signals from the NMR probe can be acquired if the carbon signal is low together with the long time required for measuring the ^{13}C DP spectra. At a magnetic field of 7 T, the direct ^{13}C polarization spectrum of the CQDs only shows the graphitic segment sp^2 at a chemical shift of 128.3 ppm (signal 1, Fig. 3A), however if the spectrum is recorded at 14 T, the spectrum presents additional signals at 113.7 and 164.7 ppm, assigned to lactol-type carbon coming from five- and/or six-membered lactol ring (signal 2, Fig. 3C-D) [36] and ester carbonyl carbon or carboxylic acid group (-CO-O-R or -CO₂H, signal 3, Fig. 3C-D) according with previous results in graphite oxide materials (Fig. 3B) [15].

Even when the spectrum B in Fig. 3 has a low S/N, the information obtained is of importance, since bulk structural information of the GQDs were achieved, but it need to be complement with the results from other spectroscopic techniques that will be discussed throughout the manuscript. The fluorine covalently bonded to the GQDs particle demonstrated from the XPS results cannot be observed in the ^{13}C ss-NMR spectra since the coupling between ^{13}C and ^{19}F affect the intensity of these resonance signals, preventing the visualization of the chemical shift for ^{13}C bounded to ^{19}F .

To gain more insight about the different surface functionalization of the materials, the samples were analyzed by temperature programmed desorption coupled to mass spectrometry, TPD-MS (Fig. S3A). The main differences in the TPD-MS profiles (Fig. S3B) correspond to the evolution of CO between 400–800 °C, with two remarkable peaks detected for the CQDs (attributed to the decomposition of phenol and carbonyl moieties in different configurations) [24], but not observed in the pristine graphite. The profiles corresponding to the loss of water (m/z 18) are also clearly different; the first peak observed for the graphite at around 150 °C is associated to the desorption of physisorbed water. The release of water above 200 °C was more intense in the case of the quantum dots; this should be associated to the decomposition of labile O-containing functional groups and/or to water formed during the reaction between two adjacent oxygen functionalities at high temperature. All this indicates that the edges of the graphene layers in the CQDs are decorated with O-surface groups different than those of the pristine graphite, mainly phenol and carbonyl type.

Excitation and emission spectra for CQDs are shown in Fig. 4A-B. Starting graphite material alone did not show any emission. It is

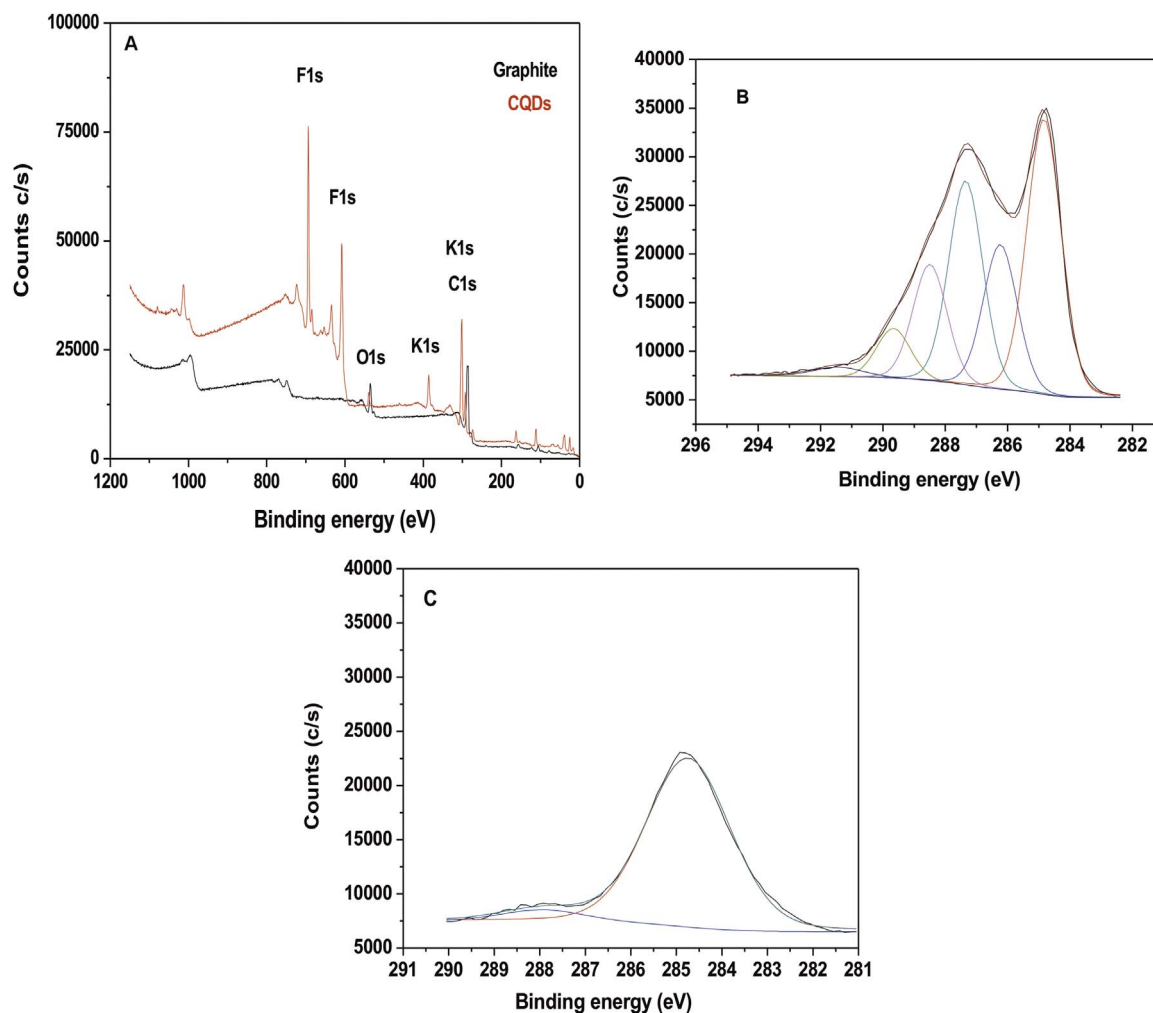


Fig. 2. A) Survey XPS spectra and deconvoluted peaks recorded for GQDs and graphite, B) C 1 s core level of graphite: 284.85 eV (C-C, sp^2); 286.13 eV (C-OH); 287.56 eV (C-O-C); 288.81 eV (H-O-C-O). (C) C 1 s core level of CQDs.

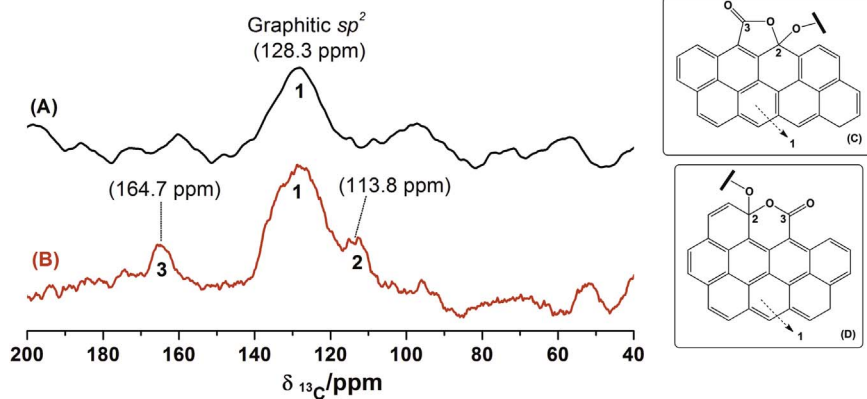


Fig. 3. ^{13}C direct polarization spectra for the CQDs particles measured at a ^{13}C frequency of 75 (A) or 150 MHz (B). The spinning rate was 10 (A) or 15 kHz (B), respectively. Partial chemical structure of the CQDs particles where the five- (C) and six membered lactol ring (D) are present together with the graphitic sp^2 regions.

obvious that both excitation and emission spectra are finely structured. The differences between neighboring maxima are about 5–6 nm (both in excitation and emission spectra), showing that the energetic differences between the corresponding vibration levels are about 300 nm. This shows that this fine spectral resolution may originate from the states in the crystal lattice of the compound.

The position of the emission maxima did not change with changing excitation wavelength, meaning that there are no additional fluorophores. This is corroborated by the result of MCR-ALS analysis, showing that the emission spectra contain only one component

(Fig. 4C). The different observed bands can be linked to the presence of various oxygen based groups. As shown by XPS and FTIR analysis, the surface of CQDs is rich in different oxygen containing groups.

3.2. Application as electrodes for electrochemical detection of dopamine and uric acid

Following the chemical and structural characterization shown above, the focus was shifted towards the electrochemical application of the prepared CQDs for the modification of electrodes and the detection

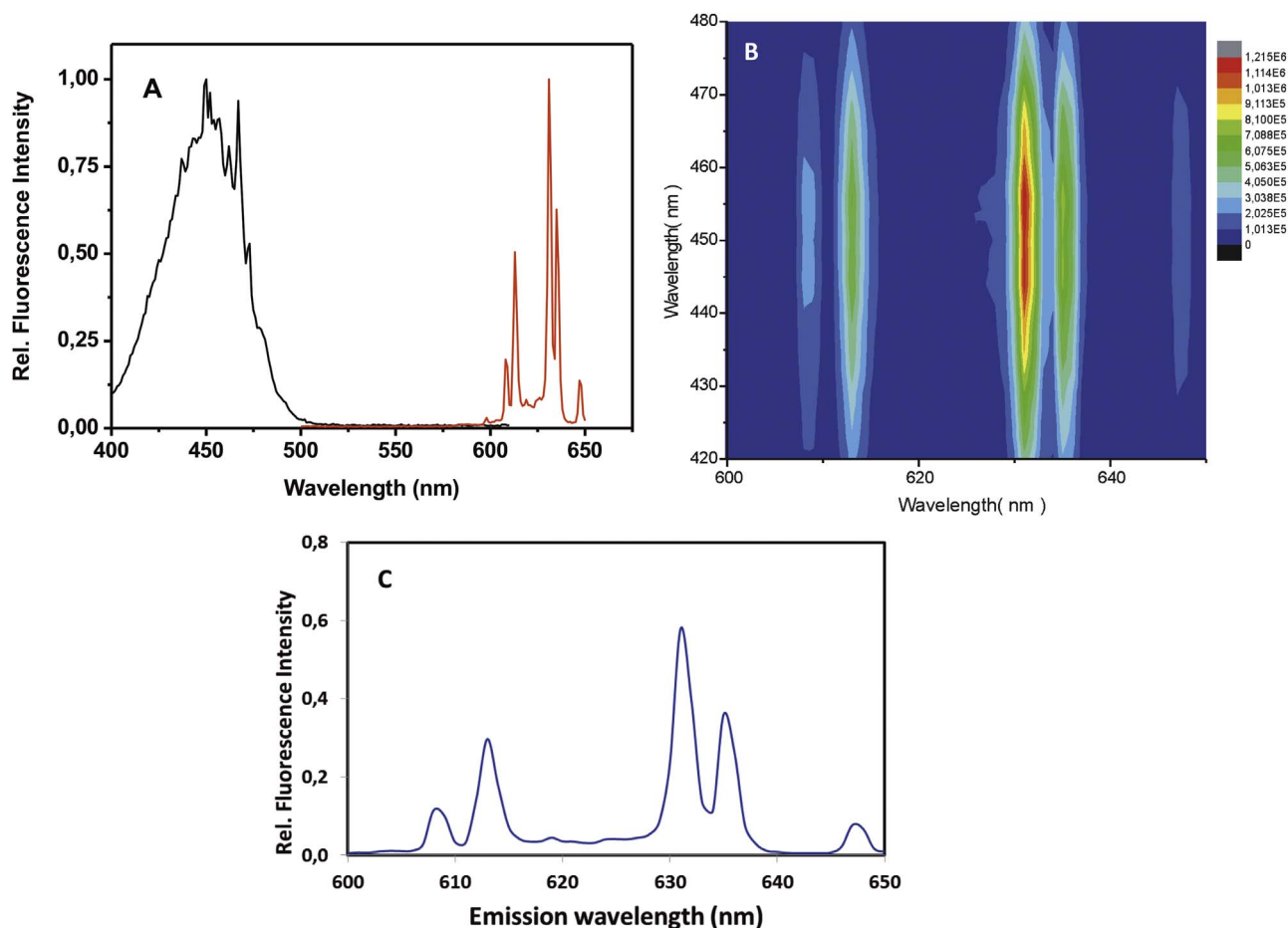


Fig. 4. A) Excitation spectrum for emission at 635 nm and emission spectrum for the 450 nm excitation; B) Fluorescence contour map for the series of emission spectra of CQDs; (C) Estimated emission profile for CQDs, as deduced from the MCR-ALS treatment.

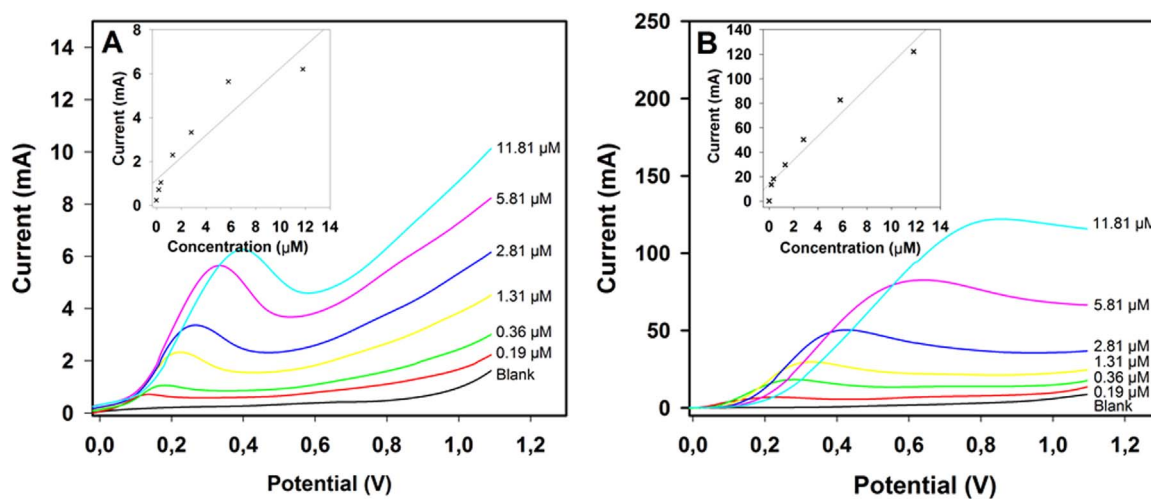


Fig. 5. Cyclic voltammograms of dopamine when using (A) bare glassy carbon electrode and (B) CQDs-glassy carbon under the previously stated conditions. Inset in (A) and (B): Calibration curve for the respective sensors.

of dopamine in presence of uric acid as interferent, both analytes of biological interest. Fig. 5 shows the linear voltammograms of a calibration set for dopamine using both bare and CQDs-modified glassy carbon electrodes (GCE). As seen, the dopamine oxidation peak in the glassy carbon electrode (GCE) appears at about +0.2 V vs Ag/AgCl; as the dopamine concentration increases the peak shifts to higher potentials due the fouling of the electrode surface. In the case of the CQDs-GCE, the oxidation potential for dopamine oxidation shifts slightly

towards higher anodic values (ca. +0.6 V), while the current is about ten times higher than that obtained for the bare GC electrode. The anodic shift in the potential indicates that the CQDs-GCE is more affected by the fouling effect than the bare GC.

The results obtained for uric acid are shown in Fig. 6. The electrochemical response of both electrodes was very similar to that obtained in the case of dopamine. In the bare GC electrode, the signal corresponding to the oxidation of uric acid appears at potentials of ca. +0.2

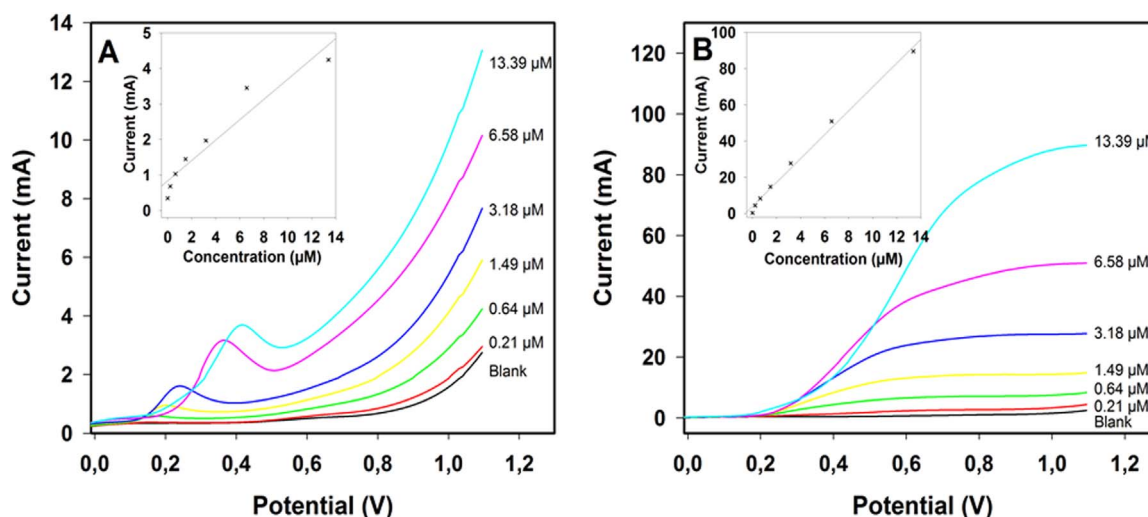


Fig. 6. Cyclic voltammograms of uric acid when using (A) bare glassy carbon electrode and (B) CQDs-glassy carbon under the previously stated conditions. Inset in (A) and (B): Calibration curve for the respective sensors.

Table 1

Calibration data for the determination of the test analytes at the stated conditions.

		Regression	R ²	Linear range (μM)	Sensitivity (mA μM ⁻¹)	LOD (μM)	LOQ (μM)
Dopamine	GCE	$y = 0.47x + 1.44$	0.844	0.19 – 11.81	0.47	7.1	21.5
	CQDs-GCE	$y = 9.3x + 18.1$	0.974	0.19 – 11.81	9.3	2.7	8.1
Uric acid	GCE	$y = 0.270x + 0.993$	0.923	0.21 – 13.39	0.27	2.01	5.5
	CQDs-GCE	$y = 6.45x + 5.27$	0.996	0.21 – 13.39	6.5	1.3	3.8

Table 2

An overview on recently reported nanomaterial-based methods for simultaneous determination of dopamine and uric acid.

Modification of electrode	Method applied	LOD DA	LOD UA	References
GCE modified with MoS ₂ and PEDOT nanocomposite	DPV	0.52 μM	0.95 μM	[37]
GCE modified with electroreduced graphene oxide and imidazolium groups	DPV	0.03 μM	5 μM	[38]
GCE modified with porous Cu ₂ O nanospheres on reduced graphene oxide	DPV	15 nM	112 nM	[39]
GCE modified with the nickel(II)-bis(1,10-phenanthroline) complex and single-walled carbon nanotubes	DPV	1 μM	0.76 μM	[40]
GCE modified with a nickel(II) norcorrole complex and MWCNTs	DPV	0.1 μM	0.4 μM	[41]
GCE modified with a hierarchical nanoporous platinum-copper alloy	DPV	2.8 μM	5.7 μM	[42]
Oxidized silicon modified with MWCNTs doped with boron	CV	0.11 μM	0.65 μM	[43]
GCE modified with CQDs	LSV	2.7 μM	1.3 μM	This work

DA: Dopamine; UA: Uric acid; MWCNTs: multi-walled carbon nanotubes; DPV: Differential Pulse Voltammetry; CV: cyclic voltammetry; LSV: Linear Sweep Voltammetry.

to +0.4 V vs. Ag/AgCl, clearly overlapping with the signal corresponding to dopamine (Fig. 5). Meanwhile for the CQDs-GCE, the value for the detection of uric acid shifted towards more positive values, although the signal was quite ill-defined with no clear observation of a peak. Also, the electrochemical response of uric acid in the CQDs-GCE electrode gave a more intense signal than that recorded for the bare GC electrode. However for both electrodes the fouling is significant at the highest concentrations tested. More interestingly, a remarkable increase in the current peak was obtained for the detection of uric acid, which results in a better sensitivity of the functionalized electrodes, almost 10 times higher, towards the analytes. Associated repetitivity (1 ppm) estimates derived from the regression lines were in the case of uric acid 4.9%RSD and 2.1%RSD for GC and CQD-GC electrodes, respectively. In the case of dopamine, repetitivities were 7.4% and 4.3%, for GC and CQD-GC electrodes, respectively.

Table 1 summarizes the calibration curves obtained for dopamine and uric acid respectively; as seen, lower limits of detection were obtained in the CQDs-GCE. While the literature reports electrocatalytic properties towards the oxidation of uric acid [20] with CQDs-GCE, the authors have only observed an increase in the current peak; this observation was also reported in similar sensing strategies [19], due to the

increase of the electrode active area. Nevertheless, the CQDs have proved to be an interesting choice that displays with clear improvement of the electrochemical properties, at least in the observed current intensity, achieving similar LOD recently reported in the literature (Table 2).

4. Conclusions

Carbon quantum dots have been synthesized through a green chemistry process, a modified Hummer's method. The resulting material has been characterized by TEM microscope, which showed a regular spherical shape and by XPS, Raman, solid-state NMR and FTIR-ATR spectroscopy demonstrating the different functionalization on the surface. Finally, the feasibility of a CQDs-GCE sensor was demonstrated with the functionalization of a glassy carbon electrode. The CQDs were employed to functionalize a GC electrode without any binding reagent; dopamine and uric acid were used as test analytes. The electrochemical detection of both compounds exhibited a high increase in the current peak in the CQDs-GCE as compared to the bare glassy carbon, although still in both cases a high fouling effect was observed on the surface. Notwithstanding, the CQDs-GCE exhibited a better sensitivity,

almost 10 times higher than the bare GC electrodes, bringing about a lower LOD for both species. The synthesized CQDs have proved to be good choice to functionalize in a simple manner a GC electrode to obtain an enhanced response towards the model analytes.

Acknowledgments

The authors thank the Ministry of Education, Science and Technology of the Republic of Serbia (grant N° 173017). JMLM thanks to ANPCYT (PICT 2012-0151), Univ. Buenos Aires (UBACyT 2013-2016/043BA) and CONICET (PIP 2014-2016/130). MV, AGC and COA thank the Spanish MINECO (grants CTQ2013-41577-P, CTQ2015-68951-C3-3-R and CTM2014/56770-R). Thanks to M. Laurenti (Complutense University of Madrid) for providing TEM images.

Appendix A. Supporting information

Supplementary data associated with this article can be found in the online version at <http://dx.doi.org/10.1016/j.talanta.2017.09.082>.

References

- [1] X. Xu, R. Ray, Y. Gu, H.J. Ploehn, L. Gearheart, K. Raker, W.A. Scrivens, *J. Am. Chem. Soc.* 126 (2004) 12736.
- [2] A. Rahy, C. Zhou, J. Zheng, S. Park, M.J. Ki, I. Jang, S.J. Cho, D.J. Yang, *Carbon* 50 (2012) 1298.
- [3] Q.L. Zhao, Z.L. Zhang, B.H. Huang, J. Peng, M. Zhang, D.W. Pang, *Chem. Comm.* 41 (2008) 5116.
- [4] S.C. Ray, A. Saha, N.R. Jana, R. Sarkar, *J. Phys. Chem. C* 113 (2009) 18546.
- [5] M. Algarra, B.B. Campos, K. Radotić, D. Mutavdžić, T. Bandoz, J. Jiménez-Jiménez, E. Rodríguez-Castellón, J.C.G. Esteves da Silva, *J. Mater. Chem. A* 2 (2014) 8342.
- [6] M. Algarra, M. Pérez-Martín, M. Cifuentes-Rueda, J. Jiménez-Jiménez, J.E. da Silva, T. Bandoz, E. Rodríguez-Castellón, J.T. López Navarrete, J. Casado, *Nanoscale* 6 (2014) 9071.
- [7] J. Wang, J. Qiu, *J. Mater. Sci.* 51 (2016) 4728.
- [8] X. Yu, J. Liu, Y. Yu, S. Zuo, B. Li, *Carbon* 68 (2014) 718.
- [9] G. Hong, S. Diao, A.L. Antaris, H. Dai, *Chem. Rev.* 115 (2015) 10816.
- [10] M. Zheng, S. Ruan, S. Liu, T. Sun, D. Qu, H. Zhao, A. Xie, H. Gao, X. Jing, Z. Sun, *ACS Nano* 9 (2015) 11455.
- [11] S.Y. Lim, W. Shen, Z. Gao, *Chem. Soc. Rev.* 44 (2015) 362.
- [12] J.C.G. Esteves da Silva, H.M. Gonçalves, *Tr. Anal. Chem.* 30 (2011) 1327.
- [13] M. Acik, G. Lee, C. Mattevi, A. Pirkle, R.M. Wallace, M. Chhowalla, K. Cho, Y. Chabal, *J. Phys. Chem. C* 115 (2011) 19761.
- [14] W. Cai, R.D. Piner, F.J. Stadermann, S. Park, M.A. Shaibat, Y. Ishii, D. Yang, A. Velamakanni, S.J. An, M. Stoller, J. An, D. Chen, R.S. Ruoff, *Science* 321 (2008) 1815.
- [15] W. Gao, L.B. Alemany, L. Ci, P.M. Ajayan, *Nat. Chem.* 1 (2009) 403.
- [16] H.W. Spiess, *Macromolecules* 43 (2010) 5479.
- [17] P.E.W. Simon, R. Ulrich, H.W. Spiess, U. Wiesner, *Chem. Mater.* 13 (2001) 3464.
- [18] B.B. Campos, R. Contreras-Cáceres, T.J. Bandoz, J. Jiménez-Jiménez, E. Rodríguez-Castellón, J.C.G. Esteves da Silva, M. Algarra, *Carbon* 106 (2016) 171.
- [19] Q. Huang, S. Hu, H. Zhang, J. Chen, Y. He, F. Li, W. Weng, J. Ni, X. Bao, Y. Lin, *Analyst* 138 (2013) 5417.
- [20] C.S. Lim, K. Hola, A. Ambrosi, R. Zboril, M. Pumera, *Electrochem. Comm.* 52 (2015) 75.
- [21] L. Zhang, Y. Han, J. Zhu, Y. Zhai, S. Dong, *Anal. Chem.* 87 (2015) 2033.
- [22] W.S. Hummers Jr., R.E. Offeman, *J. Am. Chem. Soc.* 80 (1958) 1339.
- [23] J. Mendieta, M.S. Díaz-Cruz, M. Esteban, R. Tauler, *Biophys. J.* 74 (1998) 2876.
- [24] T.J. Bandoz, C. Ania, *Sci. Technol.* 7 (2006) 159.
- [25] J. Figueiredo, M. Pereira, M. Freitas, J. Orfao, *Carbon* 37 (1999) 1379.
- [26] B.M. Fung, A.K. Khitrin, K. Ermolaev, *J. Magn. Reson.* 101 (2000) 97.
- [27] Y. Xu, H. Bai, G. Lu, C. Li, G. Shi, *J. Am. Chem. Soc.* 130 (2008) 5856.
- [28] J. Coates, *Interpretation of Infrared Spectra, a Practical Approach*, Encyclopedia of Analytical Chemistry, John Wiley & Sons Ltd, Chichester, 2000.
- [29] A.C. Ferrari, J. Robertson, *Phys. Rev. B* 61 (2000) 14095.
- [30] M. Vázquez-Nakagawa, L. Rodríguez-Pérez, M.A. Herranz, N. Martín, *Chem. Comm.* 52 (2016) 665.
- [31] Y. Guo, X. Sun, Y. Liu, W. Wang, H. Qiu, J. Gao, *Carbon* 50 (2012) 2513.
- [32] K. Haubner, J. Murawski, P. Olk, L.M. Eng, C. Ziegler, B. Adolphi, E. Jaehne, *Chem. Phys. Chem.* 11 (2010) 2131.
- [33] R. Nair, M. Sepioni, I.L. Tsai, O. Lehtinen, J. Keinonen, A. Krashennnikov, A.V. Krashennnikov, T. Thomson, A.K. Geim, I.V. Grigorieva, *Nat. Phys.* 8 (2012) 199.
- [34] I. Jung, D.A. Field, N.J. Clark, Y. Zhu, D. Yang, R.D. Piner, S. Stankovich, D.A. Dikin, H. Geisler, C.A. Ventrice Jr., R.S. Ruoff, *J. Phys. Chem. C* 113 (2009) 18480.
- [35] J.M. Lázaro-Martínez, E. Rodríguez-Castellón, D. Vega, G.A. Monti, A.K. Chattah, *Macromolecules* 48 (2015) 1115.
- [36] A.F. Crespi, D. Vega, A.K. Chattah, G.A. Monti, G.Y. Buldain, J.M.L.ázaro-Martínez, *J. Phys. Chem. A* 120 (2016) 7778.
- [37] Y. Li, H. Lin, H. Peng, R. Qi, C. Luo, *Microchim. Acta* 183 (2016) 2517.
- [38] F. Wu, T. Huang, Y. Hu, X. Yang, Y. Ouyang, Q. Xie, *Microchim. Acta* 183 (2016) 2539.
- [39] L.P. Mei, J.J. Feng, L. Wu, J.R. Chen, L. Shen, Y. Xie, A.J. Wang, *Microchim. Acta* 183 (2016) 2039.
- [40] S. Yan, X. Li, Y. Xiong, M. Wang, L. Yang, X. Liu, C. Zhang, *Microchim. Acta* 183 (2016) 1401.
- [41] K. Deng, X. Li, H. Huang, *Microchim. Acta* 183 (2016) 2139.
- [42] D. Zhao, D. Fan, J. Wang, C. Xu, *Microchim. Acta* 182 (7–8) (2015) 1345.
- [43] N.G. Tsierekzos, U. Ritter, Y.N. Thaha, C. Downing, P. Szroeder, P. Scharff, *Microchim. Acta* 183 (2016) 35.